Hindawi
Advances in Materials Science and Engineering
Volume 2021, Article ID 5566142, 10 pages
https://doi.org/10.1155/2021/5566142

Research Article

Study on the Influence of Tectonic Stress on Stability of Horseshoe-Shaped Tunnels

Xin Lv,[1] **Shuzhi Wang**,[2] **Yu Qiu**,[3] **and Xiangxin Liu**[2]

[1]*Modern Technology and Education Center, North China University of Science and Technology, Tangshan 063210, China*
[2]*College of Mining Engineering, North China University of Science and Technology, Tangshan 063210, China*
[3]*Sinosteel Maanshan Institute of Mining Research Co., Ltd., Ma'anshan 243000, China*

Correspondence should be addressed to Shuzhi Wang; wangszh@ncst.edu.cn

Received 16 February 2021; Revised 13 April 2021; Accepted 3 May 2021; Published 31 July 2021

Academic Editor: Fengqiang Gong

While the tunnel is in the high tectonic stress environment and surrounding rock of tunnel has the characteristics of soft texture and stronger expansion, the preference of tunnel shape is horseshoe. An elastic-plastic model is analyzed by complex function theory in accordance with the deformation characteristics of a horseshoe-shaped tunnel in an engineering site. The numerical model of the tunnel is built by FLAC3D, and the influence of the magnitude and direction of structural stress on the horseshoe-shaped tunnel is studied in detail. Finally, the security support of the tunnel is discussed. Results show that the stress concentration phenomenon is easily focused on the left, right, and bottom sides of the tunnel; these places should therefore be the focus of attention of tunnel stability analysis. The magnitude and direction of tectonic stress greatly affect the stability of the horseshoe-shaped tunnel. Similarly, the magnitude of tectonic stress can significantly affect the deformation state of the tunnel. The direction of tectonic stress mainly reflects the orientation of the tunnel. In addition, the orientation of the tunnel should be arranged along the maximum direction of principal stress.

1. Introduction

With the continuous development of economic construction, science, and technology, the development of underground space has increasingly broadened, even to the Earth's deep interior [1]. In the environment of high ground stress and high geothermal heat, rocks undergo brittle-duct or brittle-plastic transformation, and the horseshoe-shaped section is widely used in deep tunnels. The horseshoe-shaped tunnel is used in engineering sites, where the surrounding rock is soft, the top and side pressures are high, and the bottom is under pressure due to its superior loading capacity [2–6].

In some cases in the literature, the straight wall arch section is used instead of the horseshoe section mainly because of the blindness and difficulty of modeling a horseshoe-shaped tunnel. To explain the meaning of the horseshoe-shaped tunnel, Li et al. [7] and Sun et al. [8] used the lateral pressure coefficient for a thorough analysis of the field of tunnel stability. The damage section of the horseshoe-shaped tunnel starts with the meso-unit tensile. Then, the macroscopic tensile failure occurs along the direction of the maximum principal stress. Islam and Shinjo [9] used the boundary element method (BEM) to analyze the stress characteristics and deformation around the faults. The horizontal and vertical stresses influence the faults, and higher stresses are concentrated near the ends of the two faults. Sun et al. [8] investigated the floor heave and failure by the combined analyses of the acquired infrared images, video photographs, and straining field variations. The horizontal stress had a great effect on the floor heave failure, and the rock mass failure was accompanied with abnormal temperature change. Hui [10] considered dynamic testing as an impact factor behind the stability of horseshoe-shaped tunnels and studied the dynamic response of lateral blasting effect on horseshoe shape. In summary, studies on the stability of horseshoe-shaped tunnel are rare, and the magnitude and direction of tectonic stress are two important

factors affecting the stability of such tunnels. Liu et al. [11] studied the rock burst in tunnel under dry and saturated conditions and investigated the influence of water contents on rock burst in tunnel. Water softened rocks and reduced their mechanical properties, and the tunnel model in the saturated state exhibited a lower dynamic failure rate, leading to quicker static failure. Hao et al. [12, 13] studied the fracture behavior and crack propagation features of coal to evaluate the dynamic failure of coal and considered the effects of the static axial prestress and loading rate on the dynamic tensile strength and crack propagation characteristics of BD coal specimens. The AE cumulative energy is more suitable for determining crack strength and damage strength of coal reservoirs.

The horseshoe-shaped section support can be divided into two sides. One side is the original tunnel (not the horseshoe-shaped tunnel), which supports the horseshoe-shaped section in the process of lining. This research accounts for the vast majority. The other side is the original tunnel (also the horseshoe-shaped tunnel), which continues to support the horseshoe-shaped section [14, 15]. An experiment on a 40-degree inclined crack horseshoe penetrated tunnel by Peng et al. [16] revealed that the tunnel deformation and failure are asymmetric. ABAQUS can be used to study the excavation and support of horseshoe-shaped tunnels [17]. The results showed a hyperbolic function relationship between concrete support and time. FLAC3D and ANSYS were used to simulate the effect of bolt support on a horseshoe-shaped tunnel [17–19]. The perspective of horseshoe-type tunnel support is mainly single, whereas according to the complex stress distribution characteristics of the deep tunnel, the single-support method is no longer suitable for deep tunnels [20].

Therefore, the stability of horseshoe-shaped tunnel needs further studies from the aspects of magnitude and direction of tectonic stress. The research on the stability and support of circular tunnel, elliptical tunnel, and straight wall arched tunnel has been comprehensively conducted. The analysis and research on the horseshoe-shaped tunnel has yet to be further strengthened. In this study, the horseshoe-shaped tunnel was investigated by elastic-plastic mechanism. The stability of the horseshoe-shaped tunnel is discussed from the perspective of stress magnitude and direction.

2. Stability Analysis of Horseshoe-Shaped Tunnel

2.1. Model Building

2.1.1. Selection of Characteristic Parameter Value in Numerical Simulation Experiments. The transformation coefficients of the mapping functions should consider the horseshoe-shaped section as an example. The calculation conditions are shown in Table 1.

Meanwhile, the six sets of parameter values in Table 2 are imported into the software Surfer. This software can plot the contour map of stress and strain (Figure 1). As shown in Figure 1, the stress and displacement concentration appeared in the two sections of the tunnel and the bottom area of the vault. These areas can be analyzed intensively in the follow-up study. The relative distribution of stress in this area is ensured to be uniform in the discussion of the supporting effect.

2.1.2. Selection of Model Dimension. Saint-Venant's principle suggests that the stress in an object caused by a load distributed over a small area (or volume) of an elastomer is substantially only slightly further from the load-applying zone, which is related to the resultant force load and resultant moment [21–24]. The area affected by the excavation of underground cavern is generally 2 to 4 times larger than that of the cavity radius. The specific size of the model can be reasonably set according to the size of the horseshoe section.

The size is 10 cm from the left wall to the left boundary, 10 cm from the right wall to the right boundary, 10 cm from the upper boundary to the top of the vault, and 10 cm from the lower boundary to the highest point of the arch. The radius of the horseshoe lane excavated is 2 m.

2.1.3. Boundary Condition Setting. The boundary setting of the two sides and the bottom of the model is fixed, whereas the upper section is free. Compared with the tectonic stress environment, the self-weight of the model is relatively small. Thus, the gradient of the self-weight is ignored, and the upper boundary is loaded with the uniform overload methods. The concrete model and its mesh distribution are shown in Figure 2.

2.2. Selection of Calculation Parameters. The mechanical parameters of the surrounding rock around the tunnel are shown in Table 2.

2.3. Selection of the Constitutive Model. The mechanical motion of common soils and rocks (such as slope stability and underground excavation) generally adopts the Mohr–Coulomb model, which is suitable for the analysis of granular materials under monotonic loading force [25–27].

3. Results

3.1. Influence of the Magnitude of Tectonic Stress on the Stability of Tunnel. The influence of the magnitude of tectonic stress on the stability of the tunnel can be mainly reflected from the two aspects of the displacement of the tunnel and the stress distribution of the tunnel. The lateral pressure coefficient is $\lambda = 2$. The horizontal and vertical displacements of the tunnel as well as the horizontal stress and vertical stress images are recorded and discussed. The calculation data are shown in Table 3.

As shown in Figure 3, the horseshoe-shaped tunnel stress concentration mainly occurs at the joint of the four arches, and the stress concentration area at the junction of the bottom arch and the side arch is significantly larger than that of the top arch and the side arch. The stress concentration area also appears as a large displacement, which is worthwhile in the support. If the tectonic stress increases, then the

Table 1: Parameters of calculation model.

Cohesion C (MPa)	Frictional angle θ (°)	Elastic modulus E (MPa)	Poisson's ratio μ	Vertical stress P (MPa)	Horizontal stress Q (MPa)
1.5	36	10000	0.25	40	20

Table 2: Parameters of the calculation model.

Cohesion C (MPa)	Frictional angle θ (°)	Elastic modulus E (GPa)	Poisson's ratio (μ)
10.6	34	18.9	0.23

stress concentration area becomes closer to the center of the tunnel, and the stress value increases accordingly. The displacement of the two sides is evidently increased, and the joints of the four stress concentrations are enhanced.

This analysis suggests that the stress concentration at the joint of the four arches of the horseshoe-shaped tunnel is evident, thereby easily leading to instability. These four key points should be emphasized in the subsequent support simulation process to support the force resistance stress of the surrounding rock. In addition, different degrees of deformation are produced in the side wall and roof and floor, which cannot be ignored during the support process.

3.2. Influence of Tectonic Stress Direction on Tunnel Stability. The full-plane strain problem is based on the analysis of plane strain problems on surface shear and one-way compressive stress [28–30]. In the engineering field, the actual stress state of the tunnel is a three-dimensional stress, and its stress state is shown in Figure 4, where σ_1 represents the maximum horizontal stress. For studying the influence of tectonic stress direction on tunnel stability, the maximum horizontal stress and the vertical angle α of the tunnel are changed. Thus, the effects can be analyzed according to the tunnel displacement and stress distribution images of the tunnel.

The coordinates of the third-order tensor (three stresses) are transformed by the transition matrix, given that the coordinate system of the tunnel model and the known ground stress are not in the same coordinate system. The coordinate system in the tunnel is called the new coordinate system P, and the ground stress coordinate system is called the original coordinate system O [31]. The coordinate transformation of the third-order tensor is as follows:

$$[P] = L[O]L^T, \tag{1}$$

where O is the third-order tensor of the original coordinate system, P is the third-order tensor of the new coordinate system, and L is the transition matrix.

The third-order tensor of the new coordinate system is solved as follows:

$$p = \begin{bmatrix} p_{xx} & p_{xy} & p_{xz} \\ p_{yx} & p_{yy} & p_{yz} \\ p_{zx} & p_{zy} & p_{zz} \end{bmatrix} = \begin{bmatrix} \sigma_3 \cdot \cos^2 \alpha + \sigma_1 \cdot \sin^2 \alpha & \frac{1}{2}(\sigma_3 - \sigma_1) \cdot \sin 2\alpha & 0 \\ \frac{1}{2}(\sigma_3 - \sigma_1) \cdot \sin 2\alpha & \sigma_1 \cdot \cos^2 \alpha + \alpha_3 \cdot \sin^2 \alpha & 0 \\ 0 & 0 & \sigma_2 \end{bmatrix}. \tag{2}$$

In the simulation, the stress and displacement of the tunnel are analyzed at 30°, 45°, 60°, and 90°. Specific material parameters and stress parameters of the numerical simulation are shown in Table 4. The relevant parameters of the calculation model are also given in the table.

The total displacement of multiple measuring points on one line is calculated in accordance with the written Fish language to accurately evaluate the displacement data. The horizontal displacement and vertical displacement at five angles are acquired by FLAC3D 5.0. The vertical displacement of the two-point midpoint line has no research value. The horizontal displacement of the roof midpoint line and bottom midpoint line has no research value. Hence, only the horizontal displacement of the two sides and the vertical displacement of the top and bottom plates are studied. Figures 1–3 show the cloud images of the influence of the direction of tectonic stress direction on the vertical displacement of the surrounding rock of the tunnel floor, vertical displacement of the roof, and horizontal displacement of the side wall. The displacement data are exported and plotted in Figure 5.

As shown in Figure 5, the overall change trend in the top and bottom of the tunnel and side wall is the same, and the displacement is increased. The differences are that the displacement of the top plate and side wall is negative deformation (corresponding to the falling of the top plate and squeezing in the side wall, respectively), whereas the bottom plate appears to be positively deformed (corresponding to the bulging of the floor of the tunnel). When the angle between the tunnel axial and maximum horizontal stress

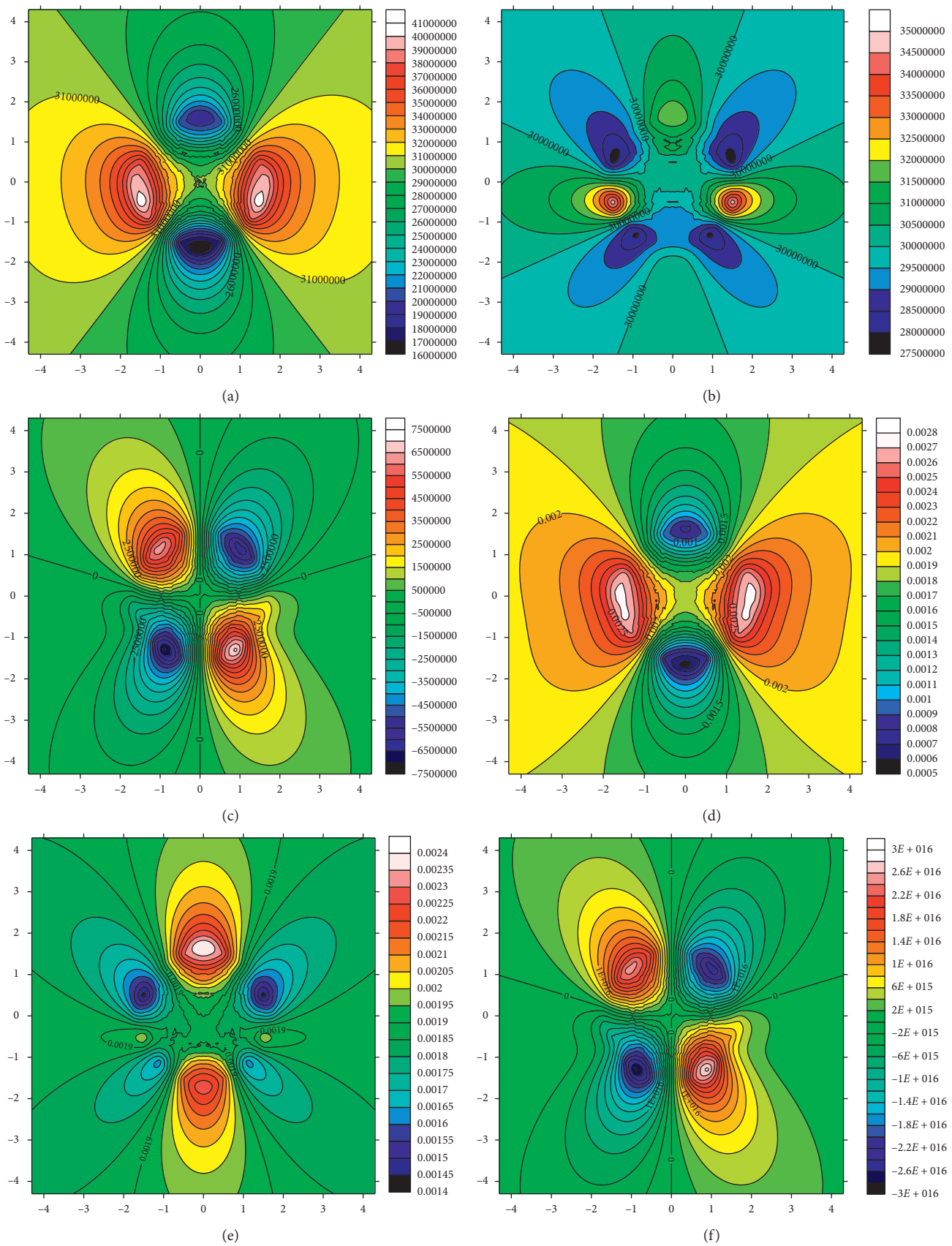

Figure 1: Contour maps of horseshoe-shaped tunnel's strain and stress. (a) Surfer contour map of σ_P. (b) Surfer contour map of σ_θ. (c) Surfer contour map of $\tau_{\rho\theta}$. (d) Surfer contour map of ϵ_ρ. (e) Surfer contour map of ε_θ. (f) Surfer contour map of $\sigma_{\rho\theta}$.

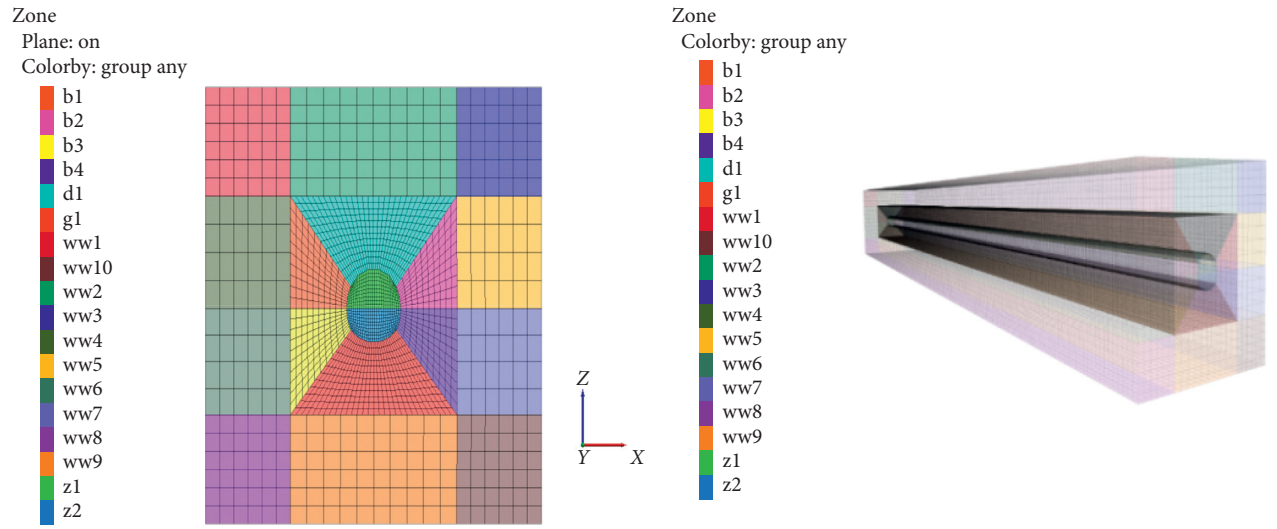

Figure 2: FLAC3D calculation model.

Table 3: Parameters of the calculation model.

Parameters	Vertical stress P (MPa)	Horizontal stress Q (MPa)
A1	10.0	20.0
A2	20.0	40.0

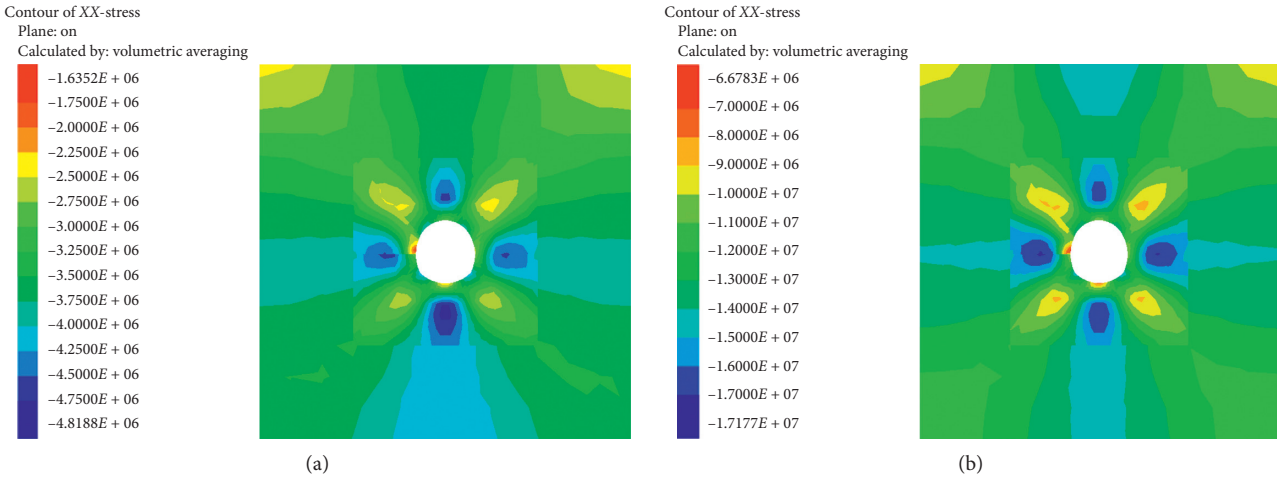

Figure 3: Continued.

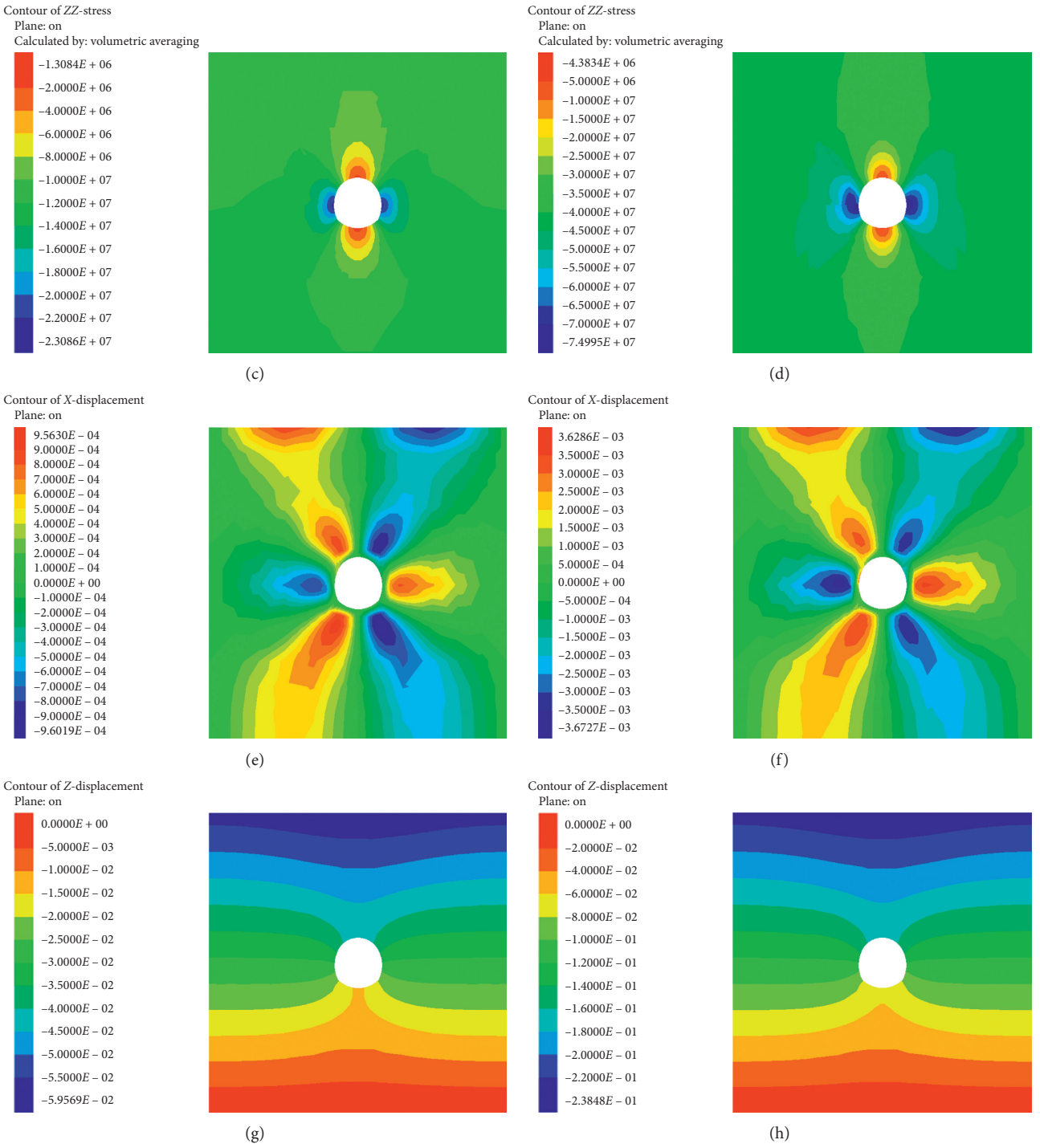

FIGURE 3: Simulation of the effect of tectonic stress on the tunnel. (a) Distribution of vertical stress ($P = 20$ MPa). (b) Distribution of vertical stress ($P = 40$ MPa). (c) Distribution of horizontal stress ($P = 10$ MPa). (d) Distribution of horizontal stress ($P = 20$ MPa). (e) Distribution of horizontal strain ($P = 20$ MPa). (f) Distribution of horizontal strain ($P = 40$ MPa). (g) Distribution of vertical strain ($P = 10$ MPa). (h) Distribution of vertical strain ($P = 20$ MPa).

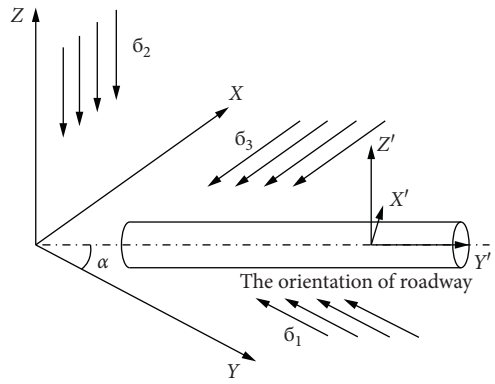

Figure 4: Actual triaxial stress state of the tunnel.

Table 4: Parameters of the calculation model.

Parameters	Angle α (°)	Cohesion C (MPa)	Frictional angle θ (°)	Elastic modulus E (GPa)	Poisson's ratio μ	σ_1 (MPa)	σ_2 (MPa)	σ_3 (MPa)
A0	0	10.6	34	18.9	0.23	20.0	8.0	5.0
A1	30	10.6	34	18.9	0.23	20.0	8.0	5.0
A2	45	10.6	34	18.9	0.23	20.0	8.0	5.0
A3	60	10.6	34	18.9	0.23	20.0	8.0	5.0
A4	90	10.6	34	18.9	0.23	20.0	8.0	5.0

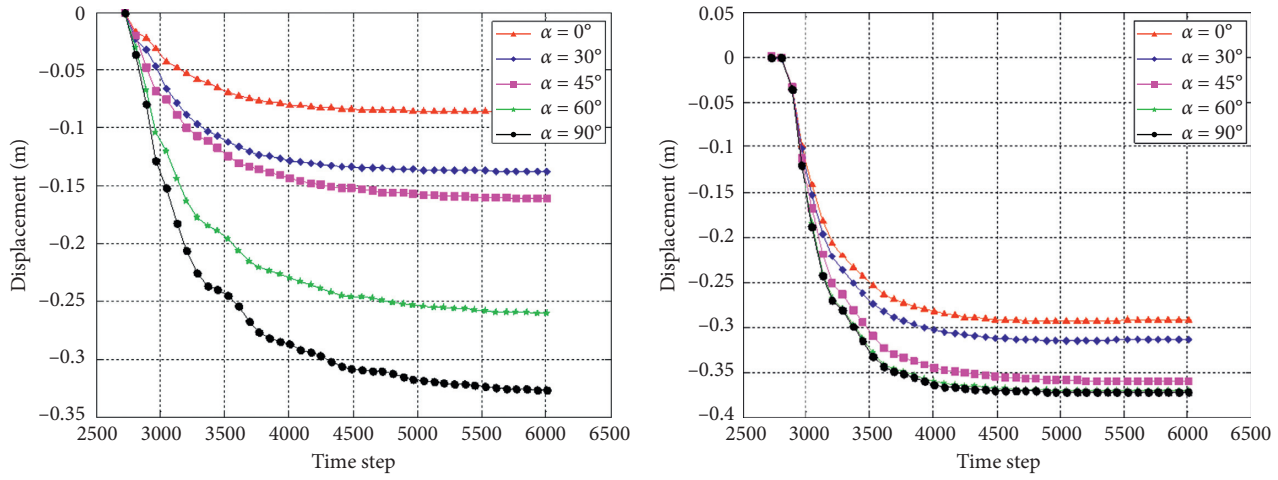

Figure 5: Continued.

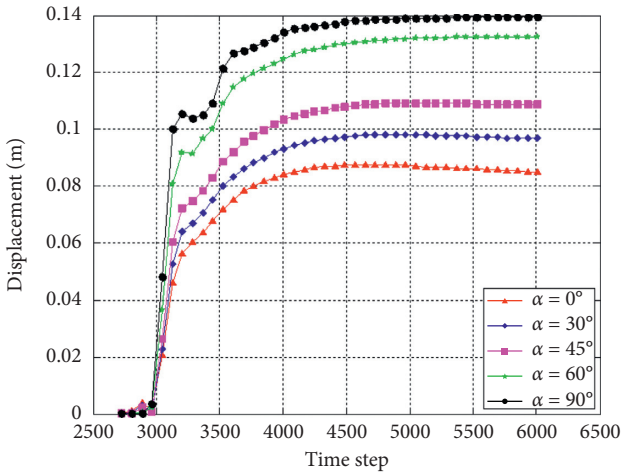

(c)

Figure 5: Simulation effect of tectonic stress direction on the tunnel. (a) Horizontal displacement of the left side. (b) Vertical displacement of the top side. (c) Vertical displacement of floor side.

increases from 0° to 90°, the displacement of the top plate is the largest, followed by the side wall, and the bottom plate is the smallest. This finding is mainly related to the geometrical dimensions of the model and the model arrangement of the four arches.

The result shows that when the tunnel axial is parallel to the maximum horizontal stress, the tunnel displacement of the key points is the smallest, which is beneficial to the stability of the surrounding rock. When the tunnel axial is perpendicular to the maximum horizontal stress, the tunnel displacement of the two sides and the top and bottom plates is the largest [32, 33]. The literature proves that when the angle between the tunnel axial and maximum horizontal stress ranges from 25° to 30°, the effect on stability of the tunnel is not evident [34].

4. Discussion

From above studies, the stress concentrations are easily caused in the place of the left, right, top, and bottom sides of tunnel. Some serious damages were happened in underground tunnels, and these destructions mainly occurred in left, right, and top sides of tunnel (Figure 6).

Shotcrete support is a support method based on the self-stability of the surrounding rock, and its main principle is embodied in four aspects, namely, support, filling, isolation, and conversion. The aim of support is to prevent the surrounding rock weathering, falling off, and form the surrounding rock as a whole. The timely injection of the initial support during excavation support is good for the subsequent installation of the anchor and the anchor cable. The anchoring depth is set to be large to anchor the lower part of the unstable rock layer to the upper stable rock layer. Prestress anchorage cable reinforcement support plays an important role in high-stress tunnel support. It can also exert prestressing, which can be applied to implement active support.

Thus, the focused monitoring areas should be actualized along the left, right, top, and bottom sides of the tunnel. In view of the complex geo-stress environment faced by deep tunnels, the three methods of combined support should be considered.

Figure 6: Rock burst in tunnel at a gold mine site [11].

5. Conclusions

(1) Stress concentration easily occurs at the left, right, and bottom sides of a horseshoe-shaped tunnel. These areas can thus be highlighted in the analysis of stability, and the uniform distribution of stress and strain in these areas is defined as the supporting effect.

(2) The impact of the direction of tectonic stress on the tunnel is mainly reflected by the selection of tunnel

orientation. Magnitude and direction of tectonic stress greatly affect the stability of horseshoe-shaped tunnels. The magnitude of tectonic stress (or lateral pressure coefficient) can significantly affect the deformation state of such tunnels.

Data Availability

The data used to support the findings of this study are available from the corresponding author upon request.

Conflicts of Interest

The authors declare that they have no conflicts of interest.

Acknowledgments

The authors gratefully acknowledge the support provided by the National Natural Science Foundation of China (NSFC) (no. 41977219) and Science and Technology Foundation of Hebei (no. 15273908).

References

[1] Q. Qian, "New progress in nonlinear mechanics-some key issues deep rock mechanics," in *Proceedings of the 8th National Rock Mechanics and Engineering Conference*, pp. 10–17, Science Press, Beijing, China, 2004.

[2] B. Jiang, L. Chen, J. S. Yang, S. Wang, and C. W. W. Ng, "Effects of twin-tunnel excavation on an existing horseshoe-shaped tunnel considering the influence of a settlement joint," *Canadian Geotechnical Journal*, vol. 54, no. 9, 2017.

[3] A. Nath and D. S. Ray, "Horseshoe-shaped maps in chaotic dynamics of atom-field interaction," *Physical Review A*, vol. 36, no. 1, pp. 431–434, 1987.

[4] C. W. W. Ng, K. Y. Fong, and H. L. Liu, "The effects of existing horseshoe-shaped tunnel sizes on circular crossing tunnel interactions: three-dimensional numerical analyses," *Tunnelling and Underground Space Technology*, vol. 77, pp. 68–79, 2018.

[5] O. N. Melnikova and K. V. Pokazeev, "Horseshoe vortices in inhomogeneous flows," *Bulletin of the Russian Academy of Sciences: Physics*, vol. 82, no. 1, pp. 69–72, 2018.

[6] Z. Jian, T. Feng, J. Yang, Y. Feng, and Y. Gao, "Upper-bound stability analysis of dual unlined horseshoe-shaped tunnels subjected to gravity," *Computers and Geotechnics*, vol. 97, pp. 103–110, 2018.

[7] Z. Li, W. Zhu, X. Feng, S. Li, H. Zho, and B. R. Chen, "Effect of lateral pressure coefficients on damage and failure process of horseshoe-shaped tunnel," *Rock and Soil Mechanics*, vol. 31, no. 2, pp. 434–441, 2010.

[8] Q. Sun, Y. Sun, Y. Liu, R. Li, and Y. Zhao, "Numerical analysis of the trajectory stability and penetration ability of different lateral-abnormal projectiles for non-normal penetration into soil based on modified integrated force law method," *International Journal of Impact Engineering*, vol. 103, pp. 159–168, 2017.

[9] M. R. Islam and R. Shinjo, "Mining-induced fault reactivation associated with the main conveyor belt roadway and safety of the Barapukuria coal mine in Bangladesh: constraints from bem simulations," *International Journal of Coal Geology*, vol. 79, no. 4, pp. 115–130, 2009.

[10] L. Hui, "The research of dynamic response characteristics for horseshoe tunnel in the case of close side blasting," *Explosion and Shock Waves*, vol. 20, no. 2, pp. 175–181, 2000.

[11] X. Liu, Z. Liang, Y. Zhang, P. Liang, and B. Tian, "Experimental study on the monitoring of rockburst in tunnels under dry and saturated conditions using AE and infrared monitoring," *Tunnelling and Underground Space Technology*, vol. 82, no. 12, pp. 517–528, 2018.

[12] H. Xianjie, W. Du, Y. Zhao et al., "Dynamic tensile behaviour and crack propagation of coal under coupled static-dynamic loading," *International Journal of Mining Science and Technology*, vol. 30, no. 5, pp. 659–668, 2020.

[13] H. Xianjie, W. Yingnan, K. Yang et al., "Anisotropy of crack initiation strength and damage strength of coal reservoirs," *Petroleum Exploration and Development*, vol. 48, no. 1, pp. 1–12, 2021.

[14] K. Hoernle, R. Werner, J. Phipps Morgan, D. Garbe-Schönberg, J. Bryce, and J. Mrazek, "Existence of complex spatial zonation in the Galápagos plume," *Geology*, vol. 28, no. 5, pp. 435–438, 2000.

[15] C. Robin, P. Mossand, G. Camus, J. M. Cantagrel, A. Gourgaud, and P. M. Vincent, "Eruptive history of the colima volcanic complex (Mexico)," *Journal of Volcanology and Geothermal Research*, vol. 31, no. 1, pp. 99–113, 1987.

[16] J. Peng, Z. Hu, Y. Men et al., "Test study of deformation and damage mechanism of horse-shoe shaped tunnel crossing ground fissure with 40°," *Journal of Rock Mechanics and Geotechnical Engineering*, vol. 28, no. 11, pp. 2258–2264, 2009.

[17] Z. Yu, P. H. S. W. Kulatilake, and F. Jiang, "Effect of tunnel shape and support system on stability of a tunnel in a deep coal mine in China," *Geotechnical & Geological Engineering*, vol. 30, no. 2, pp. 383–394, 2012.

[18] M. R. Islam and R. Shinjo, "Numerical simulation of stress distributions and displacements around an entry roadway with igneous intrusion and potential sources of seam gas emission of the Barapukuria coal mine, NW Bangladesh," *International Journal of Coal Geology*, vol. 78, no. 4, pp. 249–262, 2009.

[19] Y. C. Zhao, D. F. Lu, and Y. Chen, "Research to the influence of bolt direction on the surrounding rock," *Applied Mechanics and Materials*, vol. 353–356, pp. 1749–1752, 2013.

[20] H. Lin, "Study of soft rock roadway support technique," *Procedia Engineering*, vol. 26, pp. 321–326, 2011.

[21] A. W. Ostrycharczyk and K. A. Malo, "Parametric study on effects of load position on the stress distribution in network arch timber bridges with light timber decks on transverse crossbeams," *Engineering Structures*, vol. 163, pp. 112–121, 2018.

[22] Y. Sugimoto and K. Kageyama, "Analysis of stress distribution near a blunt surface notch tip in an orthotropic fiber under tension," *Theoretical and Applied Fracture Mechanics*, vol. 89, pp. 29–34, 2017.

[23] M. Y. Fattah, M. R. Mahmood, and M. F. Aswad, "Stress distribution from railway track over geogrid reinforced ballast underlain by clay," *Earthquake Engineering and Engineering Vibration*, vol. 18, no. 1, pp. 77–93, 2019.

[24] S. Miura, S. Kasahara, S. Yamauchi, and H. Egusa, "Effect of finish line design on stress distribution in bilayer and monolithic zirconia crowns: a three-dimensional finite element analysis study," *European Journal of Oral Sciences*, vol. 126, no. 2, pp. 159–165, 2018.

[25] M. Massoudi and M. M. Mehrabadi, "A continuum model for granular materials: considering dilatancy and the Mohr-

Coulomb criterion," *Acta Mechanica*, vol. 152, no. 1–4, pp. 121–138, 2001.

[26] H. A. Taiebat and J. P. Carter, "A semi-empirical method for the liquefaction analysis of offshore foundations," *International Journal for Numerical and Analytical Methods in Geomechanics*, vol. 24, no. 13, pp. 991–1011, 2015.

[27] J. Zhao, "Applicability of Mohr-Coulomb and Hoek-Brown strength criteria to the dynamic strength of brittle rock," *International Journal of Rock Mechanics and Mining Sciences*, vol. 37, no. 7, pp. 1115–1121, 2000.

[28] K. K. Ang and S. Valliappan, "Pseudo-plane strain analysis of wave propagation problems arising from detonations of explosives in cylindrical boreholes," *International Journal for Numerical and Analytical Methods in Geomechanics*, vol. 12, no. 3, pp. 301–322, 2010.

[29] G. Kress and M. Winkler, "Corrugated laminate analysis: a generalized plane-strain problem," *Composite Structures*, vol. 93, no. 5, pp. 1493–1504, 2011.

[30] Y. Zheng, "A simplified model of triaxial stress field around long openings," *Journal of Coal Science and Engineering*, vol. 4, pp. 76–82, 1982.

[31] Z. Xu, *Elasticity Concise Guide*, Higher Education Press, Beijing, China, 2012, in Chinese, 4th edition.

[32] T. Gentzis, "Stability analysis of a horizontal coalbed methane well in the rocky mountain front ranges of southeast British Columbia, Canada," *International Journal of Coal Geology*, vol. 77, no. 3-4, pp. 328–337, 2009.

[33] M. A. Perras, M. S. Diederichs, and D. Besaw, "Geological and geotechnical observations from the Niagara tunnel project," *Bulletin of Engineering Geology and the Environment*, vol. 73, no. 4, pp. 1303–1323, 2014.

[34] Y. Zhang, M. Cai, and Z. Ouyang, "Theoretical research on the relationship between in situ stress field and the layout of tunnel," *Geotechnical Engineering Technique*, vol. 19, no. 2, pp. 93–97, 2005.